NeuroImage 45 (2009) S86–S98

Contents lists available at ScienceDirect

NeuroImage

journal homepage: www.elsevier.com/locate/ynimg

# Discrete conformal methods for cortical brain flattening

Monica K. Hurdal [a,*], Ken Stephenson [b]

[a] Department of Mathematics, Florida State University, Tallahassee, FL 32306-4510, USA
[b] Department of Mathematics, University of Tennessee, Knoxville, TN 37996-1300, USA

ARTICLE INFO

*Article history:*
Received 15 October 2008
Accepted 15 October 2008
Available online 11 November 2008

*Keywords:*
Circle packing
Conformal map
Cortical flat map
Mapping
Riemann Mapping Theorem
Surface flattening

ABSTRACT

Locations and patterns of functional brain activity in humans are difficult to compare across subjects because of differences in cortical folding and functional foci are often buried within cortical sulci. Unfolding a cortical surface via flat mapping has become a key method for facilitating the recognition of new structural and functional relationships. Mathematical and other issues involved in flat mapping are the subject of this paper. It is mathematically *impossible* to flatten curved surfaces without metric and area distortion. Nevertheless, "metric" flattening has flourished based on a variety of computational methods that minimize distortion. However, it is mathematically possible to flatten without any *angular* distortion — a fact known for 150 years. Computational methods for this "conformal" flattening have only recently emerged. Conformal maps are particularly versatile and are backed by a uniquely rich mathematical theory. This paper presents a tutorial level introduction to the mathematics of conformal mapping and provides both conceptual and practical arguments for its use. Discrete conformal mapping computed via circle packing is a method that has provided the first practical realization of the Riemann Mapping Theorem (RMT). Maps can be displayed in three geometries, manipulated with Möbius transformations to zoom and focus on particular regions of interest, they respect canonical coordinates useful for intersubject registration and are locally Euclidean. The versatility and practical advantages of the circle packing approach are shown by producing conformal flat maps using MRI data of a human cerebral cortex, cerebellum and a specific region of interest (ROI).



## Introduction

The cortex of humans is a highly convoluted surface. The folds (gyri) and fissures (sulci) of the brain vary in size and position from person to person, and this variability has made it difficult for medical researchers to analyze and compare patterns of functional activation within and between subjects. A number of methods have been implemented that take advantage of the two-dimensional sheet topology of the cortical surface; the resulting "flat mappings" of the cerebral and cerebellar cortex may facilitate the recognition of structural and functional relationships.

This paper discusses the mathematics, computations, and application of a flat mapping approach which uses circle packings to approximate conformal maps of cortical surfaces. Such maps, termed "discrete conformal maps", are analogues of the conformal mappings of analytic function theory, allowing this rich classical theory to be exploited. Researchers will find both conceptual and practical advantages in discrete conformal mapping. The basics of classical conformal geometry and its discrete analogue are discussed. The computations and mapping tools of circle packing are illustrated by producing and manipulating discrete conformal flat maps of data from an MRI volume of the human cerebral cortex, cerebellum and a specific region of interest (ROI).

Certain technical preliminaries are involved in all flattening efforts. First is the acquisition of the initial three-dimensional (3D) data; anatomical and functional data volumes of the cerebrum can be obtained non-invasively using a variety of neuroimaging modalities, including magnetic resonance imaging (MRI), functional MRI (fMRI), and positron emission tomography (PET) (see Toga and Mazziotta, 1996 for a compilation of various methods). Data preprocessing can include intra- and intersubject registration, inhomogeneity correction, segmentation, parcellation and visualization. A common approach to visualizing functional data has been to project a focus of activation on a cross-section or slice of the brain volume. This approach suffers from a number of disadvantages due to the highly folded structure of the cortex. Activated foci that appear close together on a slice or 3D surface rendering may be quite far apart when visualized on the unfolded cortical surface. In a given individual, foci are often buried within cortical sulci and appear in a number of discrete slices, making it difficult to compare multiple foci simultaneously. Moreover, intersubject comparisons of focus location and extent are affected, inter alia, by individual differences in folding patterns (Rehm et al., 1998).

After data acquisition and preprocessing, all flattening efforts require that a finite representation of the surface region of interest be extracted from the 3D brain volume. Historically, that surface was reconstructed by tracing contours from histological sections. Wire

* Corresponding author. Fax: +1 850 644 4053.
*E-mail address:* mhurdal@math.fsu.edu (M.K. Hurdal).

1053-8119/$ – see front matter © 2008 Elsevier Inc. All rights reserved.
doi:10.1016/j.neuroimage.2008.10.045

frames or sheets were then created from the contours and these were aligned and stacked to reconstruct the surface (Rosa et al., 1997). In the last decade, a number of research groups have developed or adapted computational tools for this purpose (Dale and Sereno, 1993; Mangin et al., 1995; Drury et al., 1996; Van Essen et al., 1998; Dale et al., 1999; Fischl et al., 1999; Hurdal et al., 1999; Goebel, 2000; MacDonald et al., 2000; Wandell et al., 2000; Shattuck and Leahy, 2002; Wood et al., 2004; Tosun et al., 2006). Whatever the approach, preprocessing steps, and topological corrections involved (see section on *Cortical surface isolation*), the final result must be a representation of the cortical surface as a polygonal mesh in 3-space which is a topologically correct sphere or a disc. Only then can flattening begin.

For the purposes of this paper, the polygonal representation of the surface in 3-space is a given. The goal of flattening is to move data from that surface to a potentially more useful setting. It is a working premise, then, that the flat maps should preserve as much "information" of value as possible. With that in mind, flattening methods can be grouped into three broad categories.

### *Ad-hoc methods*

Combinatorially speaking, cortical meshes are just planar graphs, and it has been known at least since Fary that every planar graph has a straight-line embedding (i.e., flattening) (Wagner, 1936; Fary, 1948). There is, in fact, a substantial body of established embedding techniques with various target criteria, such as convexity or resolution, often having extremely efficient implementations. These methods are "ad-hoc" because they can lose information, and despite their occasional utility, they will not be considered further.

### *Metric methods*

The principal surface structures of scientific interest may seem to be "metric", referring to Euclidean lengths and areas. Several metric algorithms have been implemented, each involving some strategy for minimizing metric and/or areal distortion between the original surface and its flattened image. A surface is typically unfolded through iterative application of functions that adjust the edge lengths of the polygonal mesh; computations halt when a flat image with distortion satisfying some fitness criterion has been obtained. In many methods, auxiliary cuts are introduced in the mesh to reduce local distortion in the remainder of the image (Schwartz, 1989; Drury et al., 1996; Fischl et al., 1999; Goebel, 2000). Drury et al., 1996 use longitudinal and torsional forces so that linear and angular distortions are reduced while unfolding the surface. Fischl et al., 1999 use the gradient of a function incorporating geodesic distance and area so that linear and areal distortions are reduced. Wandell et al., (2000) use a method which begins with a graph embedding technique followed by an iterative process to reduce linear distortions. Metric flattening algorithms have been central to brain flattening efforts.

### *Conformal methods*

A companion to the metric structure on surfaces, but less familiar, is the "conformal" structure. A conformal flat map is one which preserves this structure; it preserves the angular measure between intersecting curves and respects other subtle features. "Discrete" maps can never be truly conformal. Angle is a local infinitesimal feature which can survive neither discretization of the surface (as with triangulations) nor numerical flattening of the result. The reader should be aware that all conformal flattering methods produce "$\kappa$-quasiconformal" maps, where $\kappa$ is a measure of conformal distortion.

There are two basic approaches to conformal flattening: (i) numerical methods such as partial differential equation (PDE) methods for solving the Cauchy–Riemann equations, harmonic energy minimization for solving the Laplace–Beltrami equation, and differential geometric methods based on approximation of holomorphic differentials (Angenent et al., 1999; Levy et al., 2002; Gu et al., 2004; Ju et al., 2005; Wang et al., 2006; Nie et al., 2007; Wang et al., 2007) and (ii) the circle packing methods (Hurdal et al., 1999; Bowers and Hurdal, 2003; Collins and Stephenson, 2003; Hurdal and Stephenson, 2004). Maps produced via circle packing enjoy the additional advantages of a comprehensive discrete theory which strongly parallels the well-known classical (continuous) conformal mapping theory. As continuous conformal maps encode a maximal amount of intrinsic geometric information for continuous surfaces, discrete conformal maps encode the maximal available intrinsic geometric information for discrete surfaces.

Since Ptolemy's flat map of the earth (which was actually conformal), attempts to preserve one or another geometric property underlay the myriad types of maps developed down the ages. The mathematical issues were clarified in the mid-nineteenth century: Gauss proved that it is impossible to flatten curved 3D surfaces without introducing metric and areal distortion (Polya, 1968). However, his student Riemann proved that it is possible to preserve angular, i.e., conformal, information (Riemann, 1876).

The Riemann Mapping Theorem (RMT) of 1851 established conformal structures as among the richest in mathematics: every surface with a conformal structure has an essentially unique conformal flattening. "Conformal map" is nearly synonymous with "analytic function", and hence intimately connected with "harmonic function" and the Laplace operator. The reader may recognize these as mainstays of science and engineering involved in electrostatics, heat and fluid flow, diffusion, Brownian motion and conformal field theories. Conformal structure, less intuitive but much deeper than metric structure, can provide medical researchers with an important new tool.

Conformal methods for computing planar regions typical in physics and engineering applications are now classical; Schwarz–Christoffel is perhaps the most well known (see DeLillo, 2006; Crowdy, 2007 for ongoing work), while the Kuhnau/Marshall "zipper" method (see Marshall and Rohde, 2007) is a newer numerical approach. Nevertheless, conformal mappings for *non-planar* domains remain impossible or notoriously difficult to approximate, and circle packing provides the first opening. This paper describes the Discrete version of the RMT (DRMT) and a circle packing algorithm that computes discrete conformal mappings carrying surfaces to the standard geometric spaces: the sphere, the plane, and the hyperbolic plane. The canonical nature of conformal maps, their "shape" information, unique surface-based coordinate systems with their automorphisms, and the supporting function theory are the principal advantages of conformal flattening. These all persist in the circle packing discrete theory.

The aim of this paper is to elucidate conformal methods and has two goals: first is to describe the scientific pedigree and importance of classical conformal mapping and its potential advantages in brain flattening; second is to describe the mathematics of the circle packing discrete conformal implementation and some of the difficulties that are particular to brain flattening. The section on *Conformal maps and surfaces of constant curvature* is an overview of conformal geometry and the section on *Computing conformal maps via circle packing* introduces discrete conformal maps and circle packing. The section on *Cortical surface isolation* is a brief description of cortical surface isolation and reconstruction techniques using MRI data. The resulting triangulations from the section on *Cortical flat maps* are used to produce discrete conformal flat maps in each of the three geometries. The section on *Versatility of the circle packing approach* illustrates manipulations of a simple example surface to highlight the versatility of circle packing. The *Discussion* section addresses various conformal flat mapping issues in the context of brain mapping, compares methods, and summarizes the advantages — extant and potential —

seen in the circle packing approach. Primers on key topics are provided in an Appendix.

## Conformal maps and surfaces of constant curvature

This section is an overview of surface geometry, conformal structures and maps, the three target geometries and their automorphisms. Additional details are in the Appendix.

Preliminary considerations in describing a surface $S$ in 3-space include topology, orientation and smoothness. Each surface of interest here is a topological sphere or, if it has boundary, a topological disc (i.e. connected, oriented, genus zero and with, respectively, no boundary or one boundary component) and can be thought of as a wrinkled rubber sphere or a wrinkled rubber disc, respectively. Each cortical surface has an obvious "outward" direction giving it an orientation. Regarding smoothness, cortical "surfaces" are merely finite collections of data points from which triangulated polyhedra are created. Treating these as *piecewise smooth* surfaces gives a well-developed language and full range of fundamental mathematical concepts and theory; in particular, they inherit from $\mathbb{R}^3$ a *Riemannian metric*.

The Riemannian metric on $S$ determines the three main structures pertinent to flattening: 1) metric structure, meaning lengths and areas; 2) curvature structure, related to peaks, valleys, and folds of $S$; and 3) conformal structure, reflecting angles between curves in $S$. The mathematical notions of *length*, *area*, *curvature* and *angle* on $S$ all fit naturally with native intuitions about these quantities. Note that *Gaussian* curvature is used because it is intrinsic to the surface $S$.

A *mapping* between surfaces $S_1$ and $S_2$ is a one-to-one function $f : S_1 \to S_2$ identifying each point $p$ of $S_1$ with a corresponding point $q=f(p)$ in $S_2$; the function $f$ (alternately, the image $f(S_1)$ in $S_2$) is called a *map* of $S_1$. The target surfaces for conformal maps are the three classical geometric surfaces represented by the (Riemann) *sphere* $\mathbb{S}^2 = \{(x,y,z)\in\mathbb{R}^3 : x^2+y^2+z^2=1\}$, the *Euclidean* plane $\mathbb{R}^2$, and the *hyperbolic* plane modeled as the unit disc $\mathbb{D} = \{(x,y)\in\mathbb{R}^2 : x^2+y^2<1\}$. These spaces have well-known Riemannian metrics of constant Gaussian curvature +1, 0, and −1, respectively. The term *flat map* of $S$ is generalized to mean a map from $S$ into any one of these spaces of constant curvature.

Value is often attached to the metric structure $S$ inherits from 3-space, and a mapping which preserves distance is said to be an *isometry*. However, a surface with non-constant Gaussian curvature cannot be mapped isometrically to a surface of constant Gaussian curvature; that is, *every flat mapping of a cortical surface necessarily introduces metric distortion.*

On the other hand, each of the surfaces $S$ also inherits a complementary but less familiar *conformal structure* residing in its angular data, and a mapping $f : S_1 \to S_2$ between surfaces is said to be *conformal* if it preserves conformal structure. This has a very straightforward interpretation in terms of the *angle* between curves intersecting at a point (i.e. between their tangent lines at the point), which is readily computed from the local metric data. Namely, $f$ is conformal if and only if it preserves the angle (both in its magnitude and orientation) between every pair of intersecting curves. In other words, whenever smooth curves $\gamma, \sigma$ intersect at $p$ in the domain, the angle between their images $f(\gamma)$ and $f(\sigma)$ at $f(p)$ is the same as that between $\gamma$ and $\sigma$ at $p$.

The RMT of 1851 asserts that *for every simply connected surface S having a conformal structure there is a conformal map from S onto precisely one of* $\mathbb{S}^2, \mathbb{R}^2$, or $\mathbb{D}$ (see Ahlfors, 1966). Every cortical surface can be mapped conformally onto $\mathbb{S}^2$ or $\mathbb{D}$ depending on whether it is a topological sphere or disc, respectively. The RMT also asserts that such mappings are *essentially* unique, meaning up to Möbius transformations which are a well-defined class of normalizations discussed in the Appendix. As for Euclidean maps, if $S$ is a topological disc then it has an astounding array of conformal maps; for example, one can deduce from the RMT that $S$ can be mapped conformally onto *any* region in $\mathbb{R}^2$ that is bounded by a simple closed curve.

So the first advantage of conformal flat mapping is the guarantee of existence and conditions for uniqueness. Additional advantages lie with the geometries of the classical Ssurfaces in which the maps reside. These surfaces are conveniently nested: $\mathbb{D}\subset\mathbb{R}^2$, and $\mathbb{R}^2$ is routinely identified, under stereographic projection, with $\mathbb{S}^2$ punctured at the south (or north) pole (see the Appendix). Moreover, it is

**Table 1**
Properties of the three different geometries

| Property | Description | Geometry |
|---|---|---|
| Geometric model | Sphere $\mathbb{S}^2 = \{(x,y,z) : x^2+y^2+z^2=1\}$ | Spherical |
| | Euclidean plane $\mathbb{R}^2$ or complex plane $\mathbb{C}$ | Euclidean |
| | Unit disc $\mathbb{D} = \{(x,y) : x^2+y^2<1\}$ | Hyperbolic |
| Points denoted by | $P=(x,y,z)$ | Spherical |
| | $P=(x,y)$ in $\mathbb{R}^2$ or $z=x+iy$ in $\mathbb{C}$ | Euclidean |
| | $z=x+iy$ | Hyperbolic |
| Differential element of arclength | $ds = \sqrt{dx^2+dy^2+dz^2}$ | Spherical |
| | $ds = \sqrt{dx^2+dy^2}$ | Euclidean |
| | $ds = \frac{2\lvert dz\rvert}{1-\lvert z\rvert^2}$ | Hyperbolic |
| Metric $\rho$ (distance between points) | $\rho(P_j,P_k) = \arccos(P_j\cdot P_k) = \arccos(x_jx_k+y_jy_k+z_jz_k)$ (radians) | Spherical |
| | $\rho(P_j,P_k) = \sqrt{(x_j-x_k)^2+(y_j-y_k)^2}$ | Euclidean |
| | $\rho(z_j,z_k) = \frac{1}{2}\log\left(\frac{\lvert 1-z_j\bar{z}_k\rvert+\lvert z_j-z_k\rvert}{\lvert 1-z_j\bar{z}_k\rvert-\lvert z_j-z_k\rvert}\right)$ | Hyperbolic |
| Curvature and geodesics | Curvature +1; geodesics are great circles | Spherical |
| | Curvature 0; geodesics are straight lines | Euclidean |
| | Curvature −1; geodesics are circle arcs that intersect the boundary of $\mathbb{D}$ orthogonally | Hyperbolic |
| Conformal automorphisms | $\phi : z\to\frac{az+b}{cz+d}$, $a,b,c,d\in\mathbb{C}$ with $ad-bc\neq 0$ and where $z$ is projected stereographically (full Möbius group) | Spherical |
| | $\phi : z\to az+b$, $a,b\in\mathbb{C}$, $a\neq 0$ | Euclidean |
| | $\phi : z\to e^{i\theta}\left(\frac{z-\alpha}{1-\bar{\alpha}z}\right)$, $\theta\in\mathbb{R}$, $\alpha\in\mathbb{D}$ | Hyperbolic |
| Packing condition for label R={$r_v$} | $\sum_{<v,u,w>}\arccos\left\{\frac{\cos(r_u+r_w)-\cos(r_v+r_u)\cos(r_v+r_w)}{\sin(r_v+r_u)\sin(r_v+r_w)}\right\} = 2\pi$ where this sum is over all faces $\langle v,u,w\rangle$ containing $v$ | Spherical |
| | $\sum_{<v,u,w>}\arccos\left\{\frac{(r_v+r_u)^2+(r_v+r_w)^2-(r_u+r_w)^2}{2(r_v+r_u)(r_u+r_w)}\right\} = 2\pi$ | Euclidean |
| | $\sum_{<v,u,w>}\arccos\left\{\frac{\cosh(r_v+r_u)\cosh(r_v+r_w)-\cosh(r_u+r_w)}{\sinh(r_v+r_u)\sinh(r_v+r_w)}\right\} = 2\pi$ | Hyperbolic |

convenient to identify $\mathbb{R}^2$ with the *complex* plane $\mathbb{C}$, so every point $(x,y)\in\mathbb{R}^2$ corresponds with a complex number $z=x+iy$. This gives us the advantage of a complex arithmetic which can be used in any of the three settings. Each target surface $\mathcal{T}$ has a rich family of *(conformal) automorphisms*, one-to-one conformal maps from $\mathcal{T}$ onto itself; these maps, $z\mapsto(az+b)/(cz+d), a,b,c,d\in\mathbb{C}, ad-bc\neq 0$, form a mathematical *group* under composition denoted by $\mathrm{Aut}(\mathcal{T})$. The main geometric features of each surface follow and are summarized in Table 1. More details are in the Appendix.

*The sphere*

$\mathbb{S}^2$ has constant Gaussian curvature +1. Circles are intersections of planes with $\mathbb{S}^2$; geodesics are arcs of great circles. The automorphism group, $\mathrm{Aut}(\mathbb{S}^2)$, is precisely the group $\mathcal{M}$ of all Möbius transformations of $\mathbb{S}^2$ (see Table 1). Though automorphisms map circles to circles, they do not respect circle centers and geodesics. Any triple of points of $\mathbb{S}^2$ can be mapped to any other triple by a unique element of $\mathrm{Aut}(\mathbb{S}^2)$ (see Fig. 1a).

*The plane*

The Euclidean plane, identified now as $\mathbb{C}$, has constant Gaussian curvature zero. Aut ($\mathbb{C}$) consists precisely of the *complex linear* maps (rotations, dilations, and/or translations), so each automorphism will map circles to circles, centers to centers, and geodesics to geodesics. The complex plane can be mapped to the surface of the sphere using stereographic projection. This maps both circles and straight lines of $\mathbb{C}$ to circles of $\mathbb{S}^2$.

*The disc*

The *hyperbolic plane* is a geometric surface of constant Gaussian curvature −1. Hyperbolic geometry is mathematical gem which is just now finding its way into applications. The most convenient model is the Poincarè disc. Its point set is the open unit disc in $\mathbb{C}$, namely $\mathbb{D}=\{z:|z|<1\}$, and distances between two points are measured in the metric $\rho$ defined by $\rho(z,w)=\frac{1}{2}\log\left(\frac{|1-z\bar{w}|+|z-w|}{|1-z\bar{w}|-|z-w|}\right)$. The points of the unit circle, $\partial\mathbb{D}$, while *not in* the hyperbolic plane, can be regarded as an "ideal" boundary, and hyperbolic distances grow as one approaches that boundary. Thus points $z$, $w$ which appear to one's "Euclidean" eyes as being close to one another can, if near $\partial\mathbb{D}$, be separated by a huge hyperbolic distance. In fact, any path running from a point of $\mathbb{D}$ to an ideal boundary point will have infinite hyperbolic length.

Hyperbolic circles correspond with Euclidean circles lying in $\mathbb{D}$ (though hyperbolic centers and radii are distinct from Euclidean centers and radii). Hyperbolic geodesics correspond with arcs of Euclidean circles which meet the unit circle $\partial\mathbb{D}$ in right angles. Any Euclidean circle which is internally tangent to $\partial\mathbb{D}$, called a *horocycle*, is treated as a hyperbolic circle of infinite radius with the point of tangency as its (ideal) center. Unlike in the other geometries, all automorphisms of $\mathbb{D}$ are *isometries*, so they preserve hyperbolic circles, circle centers, and geodesics.

Fig. 1b illustrates this geometry. A shaded disc of hyperbolic radius 0.4 centered at the origin, a triple of mutually tangent circles (including a horocycle) and the (hyperbolic) triangle formed by their centers, and a centered polar-coordinate-style reference grid are shown; subsequent figures show these same objects after applying the automorphism $\phi: z\mapsto(3z+1)/(3+z)$ once and twice, respectively. In each image the shaded disc has the same hyperbolic radius, though Euclidean eyes see it as getting progressively smaller as it approaches the boundary. Also the grid remains an orthogonal grid, but with a new "pole".

*Summary*

The three classical geometries form a unified and nested hierarchy. They are nested as sets, $\mathbb{D}\subset\mathbb{C}\subset\mathbb{S}^2$; their automorphisms are nested as subgroups of $\mathcal{M}$, $\mathrm{Aut}(\mathbb{D})<\mathrm{Aut}(\mathbb{C})<\mathrm{Aut}\left(\mathbb{S}^2\right)=\mathcal{M}$; and both the automorphisms and the inclusion maps preserve circles. In particular, any set $\mathbb{C}$ which is a circle in one space will necessarily be a circle in any of the other spaces which happens to contain it. Also, all the geometries are "locally Euclidean", meaning that at high magnification, the

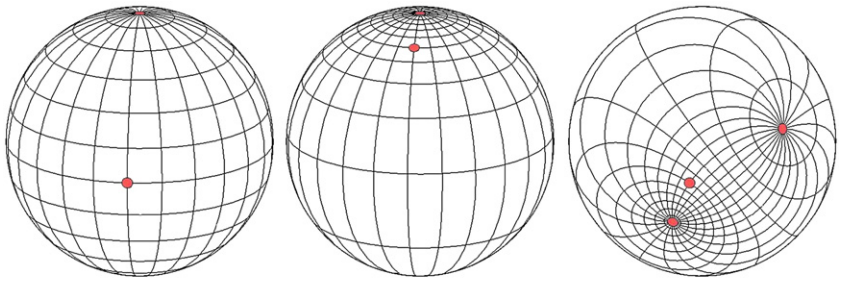

(a) Automorphisms of the sphere $\mathbb{S}^2$.

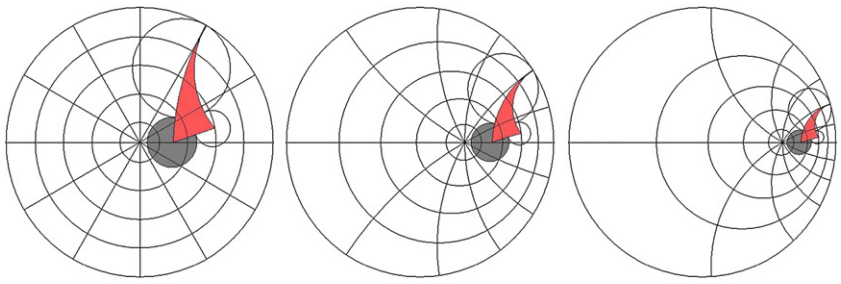

(b) Automorphisms of the hyperbolic plane $\mathbb{D}$.

**Fig. 1.** Automorphisms of the sphere $\mathbb{S}^2$ and hyperbolic plane $\mathbb{D}$. In (a): spherical map with equatorial point; Möbius transformation that shifts equatorial point only; Möbius transformation that shifts north and south poles and equatorial point. In (b): the automorphism $\phi: z\mapsto(3z+1)/(3+z)$ is applied successively. In practice, such maps allow selected regions to be brought into focus while relegating other regions to the periphery of the hyperbolic map.

neighborhood of any point looks Euclidean — small circles in the metric look like Euclidean circles, geodesics look like Euclidean straight lines, and so forth. In other words, these geometries all look locally like our familiar Euclidean world. Table 1 summarizes various properties of these geometric surfaces; see the Appendix for details.

## Computing conformal maps via circle packing

Conformal maps are guaranteed to exist by the RMT, but are impossible to compute precisely — and until recently, have not even been susceptible of approximation. However, an area of mathematics known as *circle packing*, introduced in 1985 (Thurston, 1985) with recent theoretical developments (Stephenson, 1999, 2002), provides a useful computational and theoretical framework. See Stephenson, 2005. The mathematical focus in this paper is on practical approximations of conformal maps via circle packing and their application to brain data. The resulting "discrete conformal" maps have a controlled but non-negligible level $\kappa$ of conformal distortion — technically they are $\kappa$-*quasiconformal*, as described in the Appendix. While reducing this distortion is desirable, the *discrete* conformal geometry of circle packing has such strong parallels to *classical* conformal geometry in both theory and intuition that to a large degree the advantages of conformal maps are already present in discrete versions.

Circle packing methods are quite a departure from standard numerical methods; circles bring a sort of "spontaneous" geometry to a given mesh, and this geometry is conformal in nature. A *circle packing* is a configuration of circles with a specified pattern of tangencies, and that "pattern" will be a triangular mesh associated with a cortical surface $S$ and topologically equivalent to a sphere or disc. It is important to isolate the *combinatorics* of this triangulation from its *geometry*. The triangulation is described in terms of its combinatorics $K$ and its geometric realization $V$, and is denoted $S=(K, V)$, where $K$ is a (simplicial) complex representing the connectivity of the vertices, edges, and faces, while $V$ is a set of vertex positions (points in $\mathbb{R}^3$) defining the shape of the mesh.

Given $K$, a circle packing $P$ for $K$ in one of the target surfaces $\mathcal{T}$ is a collection $\{c_v\}$ of circles in $\mathcal{T}$, one for each vertex $v$ of $K$, so that $c_v$ is tangent to $c_u$ whenever $\langle v, u\rangle$ is an edge of $K$ and so that a triple $\langle c_v, c_u, c_w\rangle$ of mutually tangent circles is positively oriented in $\mathcal{T}$ whenever $\langle v, u, w\rangle$ is a positively oriented face of $K$. Such a circle packing gives a new triangulation $S'$ lying in $\mathcal{T}$ where $S'=(K, V')$, i.e. the same combinatorics but a new set of vertex positions determined by the centers of the circles. An example is illustrated in Figs. 2a, b. Starting with the randomly generated planar surface $S=(K, V)$ in (a), a plane rectangular packing $P$ for $K$ is computed, inducing a new surface $S'=(K, V')$ in (b); the circle centers $V'$ give carr $(P)$, as described in the Appendix. Since $S$ and $S'$ share $K$, each vertex of $S$ corresponds to a vertex $v$ of $K$ and hence to a circle $c_v$ of $P$. Thus the three vertices defining any face of $S$ may be identified with the three circle centers defining a triangle in $S'$; extending to edges and faces yields a mapping $f : S \to S'$. A map defined in this way will be called a *(discrete) conformal map*. Other packings for $K$ are shown in Figs. 2c, d.

Discrete conformal maps depend on the existence of circle packings for given (extremely complicated) patterns $K$. Existence follows from results of Koebe, Andreev, and Thurston (Koebe, 1936; Andre'ev, 1970; Thurston, 1997). By treating the abstract complex $K$ as a *discrete* conformal structure on $S$, existence and uniqueness results for circle packings may be formulated in parallel with classical function theory. Thus the Discrete Riemann Mapping Theorem (DRMT) asserts that *for every simply connected triangulated surface S there is a discrete conformal map from S onto precisely one of* $\mathbb{S}^2, \mathbb{C}$, or $\mathbb{D}$. More precisely, if $K$ is a topological sphere then there exists a circle packing $P_K$ for $K$ lying in $\mathbb{S}^2$ and $P_K$ is unique up to automorphisms of $\mathbb{S}^2$, while if $K$ is a topological disc and finite, then there exists a circle packing $P_K$ for $K$ lying in the hyperbolic plane $\mathbb{D}$ for which the circles associated with boundary vertices of $K$ are horocycles, and $P_K$ is then unique up to automorphisms of $\mathbb{D}$ (e.g., Fig. 2c).

The packing $P_K$ described in the previous paragraph is called the *maximal* packing for $K$, and as noted is essentially unique. When $K$ is a topological disc, however, there exists a whole zoo of additional discrete conformal maps. For instance, if $v_1, \cdots, v_n$ denote the boundary vertices of $K$, then the Circle Packing Theorem (CPT) (Beardon and Stephenson, 1990) asserts that given any assignment of positive numbers $r_1, \cdots, r_n$ there exists a unique (up to isometry) circle packing $P$ in $\mathbb{R}^2$ or $\mathbb{D}$ such that for each $i$, $i = 1, \cdots, n$, the boundary circle $c_{v_i}$ of $P$ has the assigned radius $r_i$. Alternately, one can preassign boundary angle sums instead (see §13.2, Stephenson (2005)), giving, e.g., circle packings $P$ with rectangular carriers as in Fig. 2b. These are discrete analogues of the classical Dirichlet and Neumann boundary value problems. The flexibility provided by these Euclidean and hyperbolic manipulations will be demonstrated in later examples.

The practical question of computing the circle packings guaranteed in theory occupies the remainder of this section, with further details provided in the Appendix. Briefly, given a circle packing $P$ for triangulation $K$, the *packing process* refers to the methods for computing (i.e., approximating) the collection $R$ of *radii* for the circles (the "packing" label) and the positions of the circles' centers, the vertices of carr $(P)$. The key is the extensive system of "flat" local compatibility conditions the circles must satisfy.

The original packing process of Thurston (Thurston, 1985), implemented with efficient algorithms in Collins and Stephenson (2003), remains the most versatile. It concentrates on computing a packing label $R$ first. The curvature of a piecewise flat surface $S$ is concentrated at its vertices. In particular, an interior vertex $v$ of $S$ has a chain of contiguous neighboring vertices that form the triangular faces surrounding $v$. The *angle sum* $\theta(v)$ is the sum of the angles at $v$ in these triangles and the *curvature* is $2\pi - \theta(v)$. To "flatten" the surface at $v$ requires geometric adjustment so that $\theta(v) = 2\pi$ (360 degrees). If the geometry is associated with a label $R$ of putative radii, then $\theta(v)$ can be computed directly from the labels for $v$ and its neighbors; this yields the "packing conditions" for flatness at $v$ as specified for each of the geometries in Table 1. $R$ is a *packing label* if and only if the packing

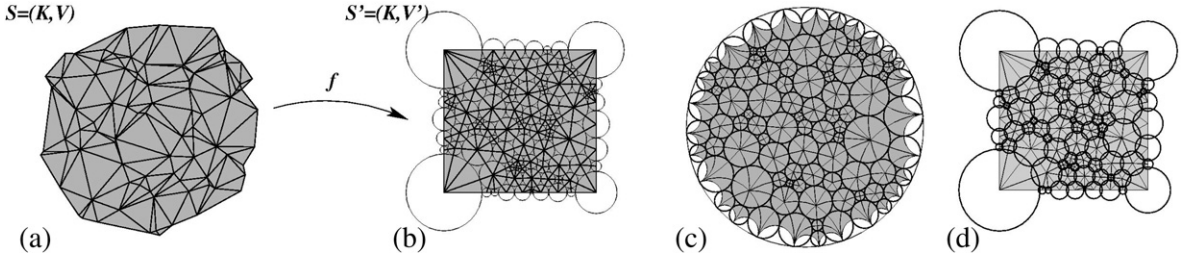


**Fig. 2.** (a) A randomly generated planar surface $S=(K,V)$, (b) a circle packing embedding $S'=(K, V')$ and the discrete conformal map $f : S \to S'$. (c) The maximal packing $P_K$ in $\mathbb{D}$, (d) an alternate rectangular "overlap" packing.

condition holds at every interior $v$. (There is (typically) no packing condition for boundary vertices, which accounts for the extra degrees of freedom a boundary provides.)

Thurston's method for finding $R$ is elegant and nicely illustrates the geometrically "spontaneous" nature of the flattening: A failure of the packing condition for a particular $v$ can be remedied by decreasing $r_v$, the radius of $v$, if the angle sum is too small (i.e. less than $2\pi$) or by increasing $r_v$ if the angle sum is too large (i.e. greater than $2\pi$). In practice, one starts a packing computation by assigning desired radii to boundary vertices (if any) and arbitrary labels (i.e. putative radii) to interior vertices. One then repeatedly readjusts the labels of the interior vertices, one at a time as described above, until the packing conditions are satisfied for all interior $v$. The boundary radii (if any) do not change. There is a comprehensive theory guaranteeing that the iterative scheme converges to a unique packing label $R$. Using the values in $R$ as radii, one easily lays out the circles to get the associated packing $P$ in the target surface $\mathcal{T}$. The packing in turn determines the associated conformal map from $S$ to $\mathcal{T}$, giving a discrete conformal flat map of $S$.

A new packing process has recently been developed by Gerald Orick, (Orick, in preparation). Exploiting geometric connections between the radii and centers of the circles, it is able to compute both simultaneously via iterative sparse matrix computations. Though it currently applies to the maximal packings only, the method is very fast, for instance, giving a packing for a spherical mesh with 250,000 vertices in just 2–3 min on a laptop.

There is no packing algorithm known to work in the spherical setting: all spherical packings are computed in $\mathbb{C}$ or $\mathbb{D}$ and then stereographically projected to $\mathbb{S}^2$. An arbitrary vertex $v_0$ and all edges containing it are removed (or punctured) from $K$, leaving a topological disc $K^*$. Its maximal circle packing $P_K$ in $\mathbb{D}$ is computed and then projected stereographically to the sphere; all its boundary circles are tangent to the equator (see Fig. 4f). The equator is introduced as the circle for $v_0$, resulting in a spherical circle packing for the original complex $K$. This circle packing is then normalized by an appropriate automorphism of $\mathbb{S}^2$, after which the choice of $v_0$ is immaterial. The above described circle packing computations are carried out with a software package called CirclePack created by Stephenson (1992–2008). See the section on *Software availability*.

The unusual nature of circle packing methods requires some comment. Packing algorithms involve "local" adjustments, each depending only on a vertex $v$ and its immediate neighbors, but the theory tells us that the consequences are ultimately global. This is, in fact, the discrete expression of the rigidity inherent in classical conformal structures and underlies the utility of the discrete methods. This rigidity, reflected in various "uniqueness" results, is a core part of the theory and should not be confused with the simple "determinism" one expects out of numerical algorithms. For instance, packings of the sphere require puncturing at some vertex $v_o$, as described above, but the result is then independent of $v_o$. In contrast, PDE methods require "pinning" one of the poles and so the choice of $v_0$ can influence the final map.

Unlike PDE conformal methods, circle packing uses only the combinatorics of a triangular mesh and not its metric structure. This seems very strange — perturbing the mesh in $\mathbb{R}^3$ does not change its flattened image. The nature of convergence of discrete maps may allay concerns. It is known, for instance, that discrete conformal flat maps converge to their classical counterparts under refinement, and that tangency packings can be generalized to inversive distance and overlap packings (as in Fig. 2(d)) to fine-tune approximations. So better absolute precision, if desired, is available — with a computational cost. A much deeper phenomenon may be in play, however. Recent circle packing experiments strongly suggest that conformality is an "emergent" phenomenon: if one *randomly* triangulates $S$ with increasingly fine meshes $K_n$, the associated discrete conformal flat maps $f_n : S \to \mathcal{T}$ (consistently normalized) appear to converge to the classical conformal map $f : S \to \mathcal{T}$ Put another way, circle packing a mesh may provide your best guess at its conformal structure — a sort of central limit phenomenon. This notion fits, for instance, with conformality's roles in recent work of Fields Medalists W. Werner on SLE (Stochastic Löwner Evolution) (Lawler et al., 2004) and A. Okounkov on random stepped surfaces (Kenyon and Okounkov, 2007).

The mathematical richness of circle packing is its strongest suit. Since the discrete model parallels classical conformality, various intrinsic behaviors (to be discussed later) are present. For example, when higher resolution MRI scans need to be incorporated into an existing database, the mathematical integrity of circle packing methods will pay dividends beyond raw approximation.

## Cortical surface isolation

In order to create a flattened map of a surface, one needs a discrete representation of that surface. For cortical data, the process of obtaining such a surface is an involved and often tedious procedure, each step the subject of numerous publications which will not be discussed in detail here. The result is a piecewise flat polygonal surface approximating the cortical surface.

All current flattening approaches require the triangulated surface to be topologically correct, i.e., a topological sphere or disc. The flat triangular faces of the surface are connected along edges and each edge is an interior edge (contained in exactly two triangles) or a boundary edge (contained in exactly one triangle). If there are no boundary edges, the surface is a topological sphere; if there are boundary edges, they form a single closed boundary component, that is, a single closed chain of edges forming the boundary, and the surface is a topological (closed) disc. Three cortical surfaces were created from MRI data as follows.

### *Human cerebral surface*

The gray matter/CSF surface representing the left cerebral hemisphere was extracted from a $1\times1\times1$ mm MRI scan of a normal human adult and parcellated into lobes. The resulting triangulation $T$ (293,840 triangles; 146,922 vertices) is a topological sphere (see Fig. 3a). To create a flat map of a topological sphere in the Euclidean or hyperbolic plane a boundary must be introduced into the surface to act as the boundary of the disc under flattening. The boundary was introduced along the corpus callosum and ventricle. Both this surface and the uncut surface are used in the conformal flattening procedure.

### *Human cerebellar surface*

This surface was selected to demonstrate that the circle packing flattening strategy applies equally well to any cortical surface. A cerebellum volume was isolated from a high-resolution T1-weighted MRI volume by stripping away the cerebrum, brainstem and cerebellar peduncles (Rehm et al., 2000) and then parcellated according to Schmahmann et al., 1999. A lobar designation or white matter label was assigned to each voxel. The cerebellar volume was heavily smoothed and an isosurface triangulated mesh of the surface was created using a marching cubes algorithm (Lorensen and Cline, 1987; Schroeder et al., 1998). The marching cubes algorithm is known to produce topological defects which were corrected semi-automatically using in-house software (Hurdal, 2008) to produce a topological 2-sphere (56,676 triangles; 28,340 vertices) (see Fig. 3e). A boundary corresponding to the white matter cut-plane and filled-in fourth ventricle was introduced where the cerebellum attached to the brainstem.

### *ROI: ventral medial prefrontal cortex and orbital frontal cortex*

The ventral medial prefrontal cortex (VMPFC) and adjacent orbital frontal cortex (OFC) are well suited to cortical flat mapping and a local coordinate system due to their highly curved geometry and complicated folding patterns. These features make morphometric analysis

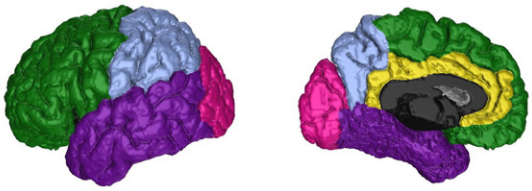

(a) Left hemisphere: lateral and medial views.

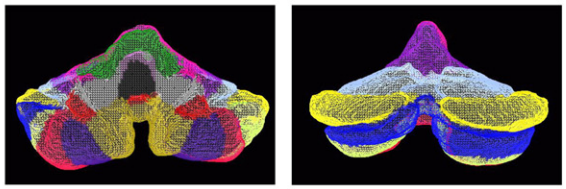

(e) Cerebellum: anterior and posterior views.

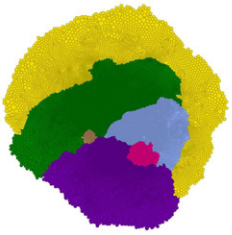

(b) Euclidean map.

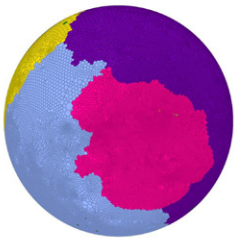

(c) Spherical map.

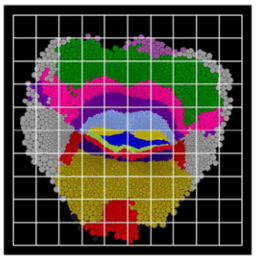

(f) Euclidean map.

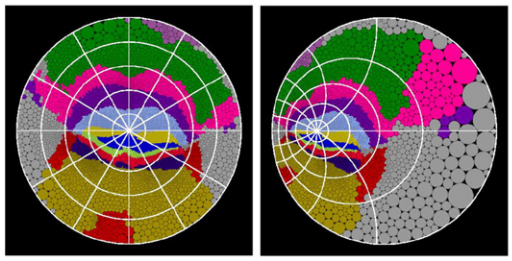

(g) Hyperbolic map with polar grid and a Möbius image.

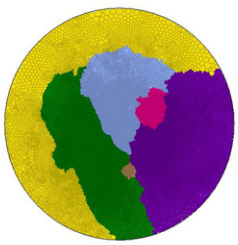

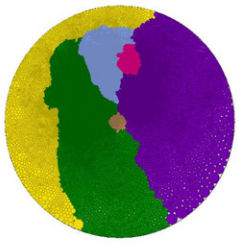

(d) Hyperbolic map and a Möbius image.

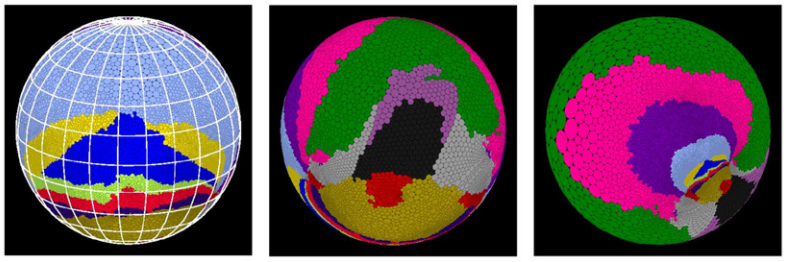

(h) Spherical map and different Möbius images.

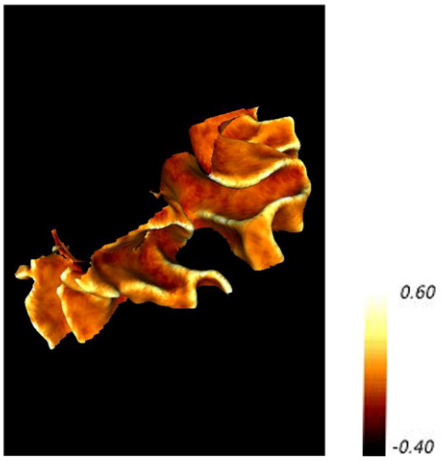


(i) VMPFC and OFC cortical surface, colored by mean curvature.

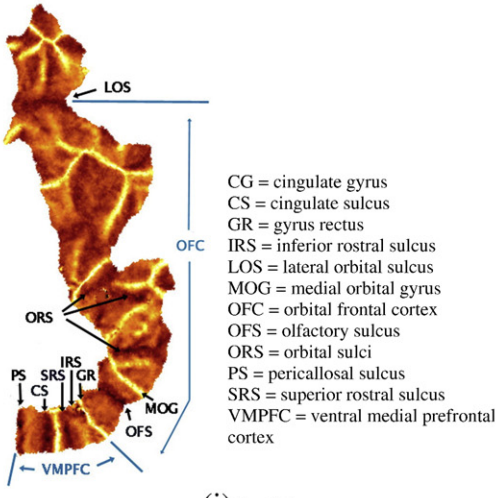


(j) Euclidean map.

**Fig. 3.** Triangulated cortical surfaces and associated conformal maps.

and visualization difficult; thus cortical flat mapping is an excellent choice for enhancing and supplementing preliminary investigations of this region. The VMPFC is located on the medial wall of the cortex and is bounded by the corpus callosum and the gyrus rectus. A topologically correct triangulated white matter surface containing the VMPFC and OFC regions was created as described in Ratnanather et al., 2001 and is shown in Fig. 3i. The surface coloring is mean curvature, with gyri (high curvature) represented with bright/white and sulci (low curvature) represented with dark/black.

## Cortical flat maps

The creation and manipulation of conformal flat maps are illustrated using the surface triangulations from the section on

*Cortical surface isolation*. Recall that after preprocessing, each complex $K$ is a topologically correct sphere or disc. One must exploit the connection with the original 3D triangulated surface $S$, each point in the flat map being associated with a point of $S$ and *vice versa*. Fundamental information resides with the surface — landmarks, standard region demarcations, surface distances, sulci, gyri, surface curvature, etc. Certain aspects of this information can be transferred to the flat map, typically using common color coding. A region or curve can be marked on the flat map, but relevant data such as surface areas and lengths, curvatures, and other metric information, must always be computed based on the connection to $S$.

The major computational effort in flattening with circle packings involves approximation of the packing radii and centers for $K$. With the latest routines these computations are quite fast, and in any case are a one-time task for a given data set; subsequent manipulations and transformations occur in real-time. The visual presentation of a circle packing flat map uses either the circles of the packing or the faces of the geometric triangulation induced by the packing (see Fig. 2). Color is used to encode additional information, such as anatomical or functional data. The original 3D surface and flat maps in any of the geometries can be viewed simultaneously. Points or regions chosen on one can be highlighted on the other.

*Euclidean maps*

The surface must be a topological disc to be flattened in $\mathbb{R}^2$. When using this scheme for flattening, each boundary vertex $w$ is assigned a label equal to the average of half the lengths of the two boundary edges containing $w$ on the original surface. Because of the boundary conditions, the resulting flat map will have the Euclidean lengths on the boundary approximately preserved. CirclePack then computes the unique packing label $R$ for $K$ having these prescribed labels for the boundary radii. Circle packings preserve conformal, not metric structure. Note that minimizing metric distortion on the boundary edges may help with visual orientation but does not imply that metric distortion is also small in the interior. In $\mathbb{R}^2$ transformations of the packings involve the Möbius transformations of Aut ($\mathbb{C}$), consisting of translations, dilations, and/or rotations, giving the user options for arbitrary real-time renormalizations in CirclePack.

Consider the surfaces described in the section on *Cortical surface isolation*. The boundary of the cerebrum consists of the boundary of the corpus callosum and ventricle and the cerebellar surface acquired a boundary when the brainstem was removed. A normalization is required before laying out the circles. For the cerebellum, the center of the horizontal fissure was placed at the origin with the base of the primary fissure vertically above the origin. For the VMPFC and OFC, the boundary corresponds to the boundary of the region. The flat maps for these surfaces are shown in Figs. 3b, f, j.

*Hyperbolic maps*

This setting also requires that the surface be a topological disc. CirclePack computes the so-called maximal packing $P_K$, which is determined by the simple requirement that the hyperbolic label must assign $\infty$ to all boundary circles, so they are horocycles in the final configuration. The cerebrum is shown in Fig. 3d and the cerebellum, repacked in $\mathbb{D}$, is in Fig. 3g and they use the same normalizations as before for the origin and a point directly above the origin (on the positive $y$-axis). Note that the enclosing outer circle represents the boundary of $\mathbb{D}$ (the unit circle), not a circle of the packing.

There are two main features to highlight regarding hyperbolic flat maps. First, the final packings all lie in a common setting (i.e. they are all disc-shaped), regardless of data set sizes, normalizations, boundary, any *ad hoc* surface cuts, and so forth. This simplifies one of the primary registration difficulties encountered with flat mappings and presents the mapping in a standard setting consistent with gathering meaningful statistics. Second is the rich group of rigid hyperbolic motions or Möbius transformations, Aut($\mathbb{D}$). The map center is of visual importance in $\mathbb{D}$ because there the map appears most Euclidean, with little hyperbolic distortion. CirclePack provides real-time interaction to bring any interior circle to the origin, allowing the map focus to be changed (see Figs. 3d, g). In Fig. 3g, the transformed coordinate grid shows the effects, with the grid lines still intersecting each other orthogonally. In other words, the view is akin to that in a light microscope: the area of interest is brought to the center and what appears to Euclidean eyes as distortion is pushed to the periphery. Recall, however, that the automorphisms are actually isometries, rigid motions in the hyperbolic sense, so these changes in focal point have absolutely no effect on any intrinsic hyperbolic structures needed for computations and statistics.

*Spherical maps*

A topological sphere $S$ cannot be mapped into $\mathbb{C}$ or $\mathbb{D}$ without introducing cuts; however, there is an essentially unique conformal map to the sphere $\mathbb{S}^2$ which is approximated with discrete conformal maps. Since there is no packing algorithm intrinsic to spherical geometry, all spherical packings are computed in $\mathbb{C}$ or $\mathbb{D}$ and then stereographically projected to $\mathbb{S}^2$, as described in the section on *Computing conformal maps via circle packing*.

Consider the data from the section on *Cortical surface isolation* which is a topological sphere. The automorphism group of $\mathbb{S}^2$ allows one to choose three points for normalization, typically points for the poles $N$ and $S$ and a point to be placed at $E$ on the equator. Figs. 3c, h display spherical packings for the cerebrum and cerebellum respectively. Fig. 3h, left, displays the spherical packing for the cerebellum with the precentral fissure mapped to $N$, the center of the horizontal fissure mapped to $S$ and the base of the primary fissure mapped to $E$. The middle figure rotates the sphere to display the location of the brain stem which was the boundary used for the other flat maps and the right figure illustrates the application of an automorphism.

*Comparisons and coordinate systems*

The normalizations required for displaying circle packings provide a means for imposing canonical coordinate systems on these flat maps. In the case of the Euclidean and hyperbolic maps, two points, such as anatomical landmarks are required, while for spherical maps it is three points (two poles and an equatorial point). The normalizations discussed in the previous sections form the basis for the coordinate grids on the flat maps in Figs. 3g, h.

It is instructive to compare the three flat maps associated with the cerebellar data by focusing in the images from Figs. 3f–h on the region near a common point, the base of the horizontal fissure. The boundary where the brain stem was removed has drastically different shapes in the three settings, but despite that one can see that the local structures in the interior are nearly identical in the three maps. The similarities would be even more striking if one focused in on a smaller region. This interior integrity despite the mapping modality is one of the key consequences of the conformal nature of the maps.

## Versatility of the circle packing approach

Circle packings provide enormous flexibility and versatility for computing flat maps. To demonstrate in an accessible way, let $S$ be the small, triangulated surface in 3-space pictured in Fig. 4a, which is a simply connected patch from Fig. 3a. The complex $K$ (211 triangles; 122 vertices including 31 boundary vertices/edges) is a topological disc, so it has a variety of packings, as illustrated by Fig. 4. Fig. 4b displays the maximal packing $P_K$ in $\mathbb{D}$ guaranteed by

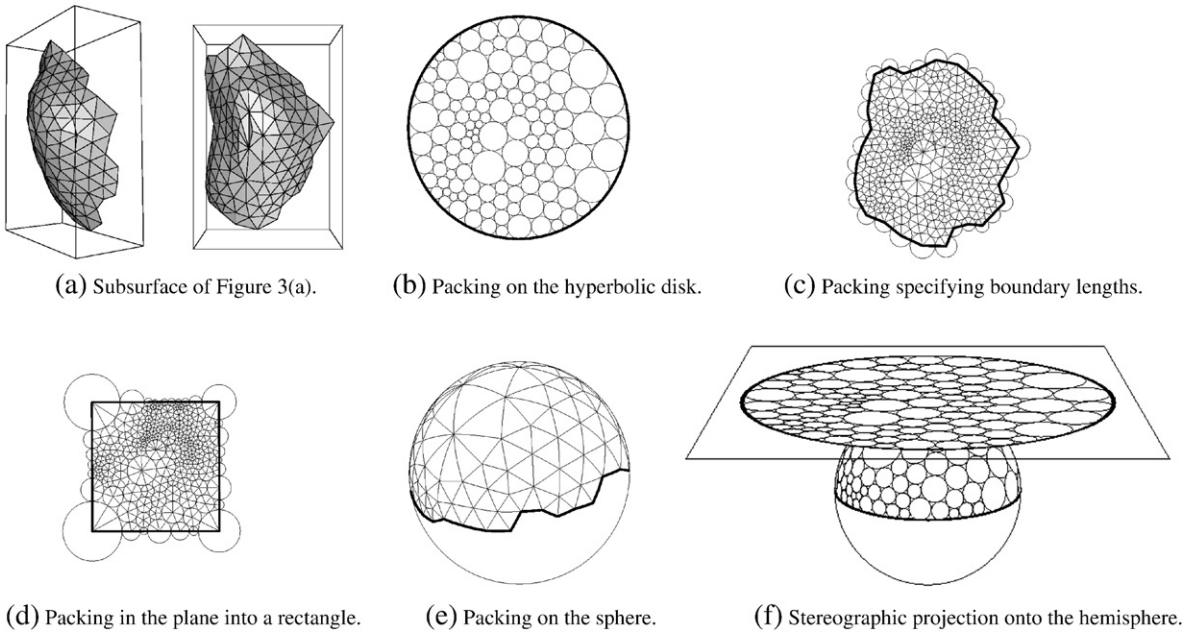


**Fig. 4.** Demonstration of conformal maps of the same complex using different packing labels.

the DRMT. Figs. 4c, d are two Euclidean packings of $K$, each with its induced triangulation for reference. In 4(c) the radii of the boundary circles were set in advance so that the lengths of boundary edges would track their lengths in $S$. Fig. 4d illustrates an alternate type of boundary condition; here the carrier was required to form a rectangle with four preselected boundary circles as its corners. Projecting Figs. 4c, b to the sphere gives the circle packings of Figs. 4e, f, respectively; Fig. 4e shows just the induced triangulation (now spherical) and Fig. 4f suggests the geometry of stereographic projection.

Properties of a surface which are preserved under conformal maps are termed *conformal invariants* and reflect something about the "shape" of $S$. (Under a $\kappa$-quasiconformal map such as provided by circle packing, an "invariant" will typically be distorted by at most a constant related to $\kappa$.) The versatility of circle packing is such that by imposing boundary conditions on the flat maps one can exploit these novel and non-intuitive measures of shape. One such conformal invariant is *extremal length*, described below.

(1) Extremal Length of Quadrilaterals: The extremal length of the rectangle $Q=[0,L]\times[0,W]$ of length $L$ and width $W$ is $EL(Q)=L/W$ (the aspect ratio of the rectangle). Rectangles $Q$ and $R$ are conformally equivalent (with "ends" identified) if and only if $EL(Q)=EL(R)$. A quadrilateral subregion $\mathcal{Q}$ of a surface with designated boundary arcs as its ends can be mapped conformally onto a unique (up to similarity) rectangle $Q$, hence one defines $EL(\mathcal{Q})=EL(Q)$. Extremal length large or small means roughly that the quadrilateral is long or wide, respectively, relative to the designated ends.

(2) Extremal Length of Annuli: The extremal length of the round annulus $A=\{(x,y):r<x^2+y^2<R\}$ is $EL(A)=\log(R/r)/2\pi$. Annuli $A$ and $B$ are conformally equivalent if and only if $EL(A)=EL(B)$. Every annular subregion $\mathcal{A}$ of a (Riemann) surface can be mapped conformally onto a unique (up to similarity) round annulus $A$, hence one defines $EL(\mathcal{A})=EL(A)$. Extremal length large or small means roughly that the annulus is fat or thin, respectively.

As an example of (1), four corner vertices of $S$ from Fig. 4a were designated as corners and $S$ was mapped to a rectangle (see Fig. 4d). Similar conformal invariants are available for annular surface regions, for relative positions of cuts, and so forth, and there exist well known extremal situations and comparison results in the mathematical literature. These conformal invariants can be thought of as a form of conformal "size" and "shape". For example, they could represent intrinsic surface information that can be exploited when comparing population groups or disease.

## Discussion: conformal mapping and brain mapping

The goal in cortical flat-mapping is to move geometric information from the cortex to a potentially more useful or complementary setting. Certain natural advantages of 2D presentations mentioned earlier accrue to all flat maps, as do standard visualization tools such as color coding, zooming, and 3D/2D display interactions. Conformal flattening methods distinguish themselves in practical terms (such as speed and versatility), scientific terms, information integrity, intuitive content and theoretical richness.

Non-conformal methods have been central to brain mapping. They tend to be fast, put one in the familiar geometries of the plane and sphere, and carry the intuitive content of lengths/areas which connect to relevant quantities, such as neuronal density and activation extent. Why consider conformal methods? The conformal methods of circle packing include all the above and additionally give notions of conformal structure and provide the world of hyperbolic geometry.

A short answer would suffice in math or physics: *existence and uniqueness*. It is impossible to preserve metric structure during flattening, whereas there's an extensive (and physically relevant) theory about maps which preserve conformal structure. In a neuroscience setting, however, more needs to be said. Because isometric flat maps do not exist, non-conformal flattening is inherently non-deterministic, with user-specified tuning parameters and stopping criteria and in some cases *ad-hoc* surface cuts. Metric intuition can be misleading as distortion is minimized only locally — global distance measurements must be done by reference to the original surface.

The three geometries used in conformal mapping have readily apparent similarities: all are locally Euclidean, have standard coordinate systems which are interrelated, and transitive subgroups of Möbius transformations for normalization, zooming and focusing.

Of course, each has its strengths. The primary advantage of a spherical map is that it requires no cuts; but of course half the image is always out of sight. Euclidean and hyperbolic maps always require a boundary, but the conformal approach does not require extraneous cuts. As with the maps of other researchers (Drury et al., 1996; Fischl et al., 1999), the shapes of circle packing Euclidean maps are largely determined by the length and number of edges in the chosen boundary and will vary from map to map. Hyperbolic maps, on the other hand, are always in the same disc, which may be a considerable advantage in registering images, making comparisons, and gathering statistics. Although hyperbolic maps may seem distorted *vis-a-vis* the Euclidean metric, Möbius transformations preserve the hyperbolic geometry while allowing the map focus to be changed interactively, relegating distortion to the map periphery. Conformal methods allow registration of only two landmarks in the Euclidean and hyperbolic cases and three in the spherical case. However, the canonical coordinate systems provide the reference grids necessary should one choose to warp images in order to align fissures, lobes, or other anatomical features.

Increasingly, conformal maps are being used in neuroscientific studies and have been shown to be just as useful, if not more so, than metric methods. Conformal brain mapping has been used in studies of the hippocampus (Gutman et al., 2007), Alzheimer's disease and schizophrenia (Thompson et al., 2004), the cerebellum (Hurdal et al., 2003), and in cortical shape matching (Gu and Vemuri, 2004; Wang et al., 2005; Lui et al., 2008) and alignment (Lui et al., 2007b). Conformal parameterizations have also been used to detect sulcal and gyral landmarks (Lui et al., 2007a). Other studies on hemispheric asymmetry (Csernansky et al., 2004), the planum temporale (Ratnanather et al., 2003), and the medial prefrontal cortex (Hurdal et al., 2003) have utilized discrete conformal maps from circle packings. Additionally, the retinotopic mapping of the visual cortex is modeled as a conformal map (Fischer, 1973; Tusa et al., 1978; Schwartz, 1980, 1994; Murray, 1989; Qui et al., 2006).

Conformal maps are associated with several classical PDE's, particularly Cauchy–Riemann, Laplace, Beltrami, and Laplace–Beltrami. Although the PDE methods share some of the conformal advantages of circle packing, they cannot handle triangulations with boundary unless the boundary is fixed *a priori* — only full spheres with one or two punctures. The authors also attach the adjective "conformal" to their maps but their maps are in fact only $\kappa$-quasiconformal. While circle packing yields bounds on $\kappa$, to our knowledge no such bounds are available in the PDE approach.

The rich theoretical framework associated with circle packing brings distinct advantages over both the metric and PDE methods. *Discrete conformal maps* are defined which both approximate conformal maps and enjoy a parallel discrete theory. In particular, they exist and are unique by the DRMT and related theorems, are computable, and can be manipulated in practice in the same ways that conformal maps can be manipulated in theory — the same canonical coordinate systems, the same Möbius transformations, the same normalizations. They also preserve the subtle conformal shape information which could well play a role in cortical studies. The comprehensive nature of the theory, taken along with the versatility and practical advantages of the resulting maps, should allow circle packing methods to keep up indefinitely with the advances and demands one can expect in the neuroscience of brain flattening.

## Software availability

The software, CirclePack, used for all computations, manipulations, and visualizations of circle packings in this paper, is available for computing packings for topologically correct surfaces (Stephenson, 1992–2008). CirclePack provides a graphical interface for displaying, manipulating, and analyzing circle packings in any of the three geometries and is written in Java for platform independence; it links to standalone C++ libraries (including Orick's algorithm (Orick, in preparation)) for more intensive computations. The software TopoCV is also available (Hurdal, 2008) for checking and correcting surfaces with topological errors before using CirclePack.

## Role of the funding sources and acknowledgements

This work and adaption of the CirclePack software for neuroscience was supported in part by NIH Human Brain Project grant P20 EB02013 and NSF grant DMS-0101329. Development of the CirclePack software has been supported in part by the National Science Foundation, NSF grant DMS-0609715. David Rottenberg (U. Minnesota) is thanked for providing the cerebellar and cerebral MRI data (acquired with funds from NIH grants R01 MH62626-01 and NS33718), as is Kelly Botteron (WUSTL) for providing the VMPFC MRI data (acquired with funds from NIH grant P41-RR15241). Agatha Lee (UCLA) is thanked for the anatomical labeling in Fig. 3j.

**Conflict of interest**
The authors declare that there are no conflicts of interest.

## Appendix

Background and additional details on the mathematics of surfaces, the classical geometric spaces, conformal maps, and circle packings follows.

### *Primer on the classical geometries*

The classical geometric spaces of constant curvature, $\mathbb{S}^2$, $\mathbb{C}$, and $\mathbb{D}$, are the most homogeneous and serve as "flat" target geometries. Their principal features are listed in Table 1. Each enjoys a *Riemannian* geometry; this is associated with a metric $\rho$ based on a differential element of arclength ds which gives lengths of curves and areas of regions as described earlier. A *geodesic*, or "straight line", segment is a shortest curve between two points, $p$ and $q$, and the distance $\rho(p,q)$ is its length. The *Gaussian curvature* for each space can be computed directly from the metric in Table 1; in each case it is constant. Angles are computed using a general version of the Law of Cosines.

Homogeneity of these spaces is reflected in their rich families of automorphisms, one-to-one conformal self-maps, all groups of Möbius transformations as indicated in Table 1. Moreover, the three geometries form a unified and nested hierarchy, $\mathbb{D}\subset\mathbb{C}\subset\mathbb{S}^2$. The last inclusion is via *stereographic projection*, so every point $z$ of $\mathbb{C}$ is identified with the point $p$ of $\mathbb{S}^2$ where the line from $z$ to the south pole of $\mathbb{S}^2$ pierces $\mathbb{S}^2$. See Fig. 4f. Stereographic projection preserves circles, angles, and orientation and respects automorphisms. Note that most texts describing stereographic projection puncture $\mathbb{S}^2$ at the north pole. If the south pole is used, the resulting stereographic map is more intuitive for the untrained user.

### *The sphere*

The distance between points is the angle (in radians) between the lines of sight of the points from the origin. It is easily deduced that a "circle" in $\mathbb{S}^2$ is the intersection of a Euclidean plane in $\mathbb{R}^3$ with $\mathbb{S}^2$ and that geodesics are arcs of great circles. In particular, this is a non-Euclidean geometry: any two straight lines intersect. Normalizing spherical maps relies on the fact that for any two triples $\{p_1,p_2,p_3\}$ and $\{q_1,q_2,q_3\}$ of points of $\mathbb{S}^2$ there exists a unique Möbius transformation $\phi\in\mathrm{Aut}\left(\mathbb{S}^2\right)$ with $\phi(p_j)=q_j, j=1,2,3$.

### *The plane*

The identification of $\mathbb{C}$ under stereographic projection with $\mathbb{S}^2$ (minus the south pole) is conformal and maps circles of $\mathbb{C}$ to circles of $\mathbb{S}^2$, though it does not respect centers. Straight lines in $\mathbb{C}$ are generally

treated as circles "going through infinity" because they correspond under stereographic projection to circles in $\mathbb{S}^2$ containing the south pole.

*The disc*

The richness of hyperbolic geometry is explained in part by the fact that automorphisms preserve hyperbolic distance. Thus images of circles are circles, images of geodesics are geodesics. Direct computation with $ds = 2|dz|/\left(1-|z|^{2)}\right.$ shows that for $z\in\mathbb{D}$, the Poincarè distance to the origin is $\rho(0,z) = (1/2)\log((1+z)/(1-z))$. So circles centered at the origin and geodesics through the origin are just Euclidean circles and Euclidean straight lines, respectively. Other circles and geodesics are images of these so, for instance, geodesics are always arcs of Euclidean circles which are orthogonal to the unit circle. Hyperbolic geometry is a second type of non-Euclidean geometry: given a line $L$ and a point $q$ not on $L$, there are infinitely many lines through $q$ parallel to $L$.

*Primer on surfaces*

The surfaces $S$ of this paper are polyhedral topological spheres or discs defined by triangular meshes. Typical topological problems — edges occurring more than twice, disconnected pieces, etc. — are detected and repaired by examining the surface complex $K$. So-called *handles* are more difficult, but can be detected using topological invariants; a surface's *Euler characteristic* $\chi(S)$ is defined by $\chi(S)=v-e+t$, where $v$, $e$, $t$ are the numbers of vertices, edges, and triangles, respectively, in $K$ (Armstrong, 1983, Massey, 1967). The number $m(S)$ of boundary components can be computed from $K$. The *genus* $g(S)$, the number of handles, satisfies $\chi(S)=2-2g(S)-m(S)$. Thus, assuming $S$ is topologically correct, has at most one boundary component, and is simply connected (so $g(S)=0$) then $S$ is a topological sphere if and only if $\chi(S)=2$ and a topological disc if and only if $\chi=1$.

Since such surfaces lie in 3-space and are piecewise flat, they inherit a Riemannian metric from $\mathbb{R}^3$. Although they lack the homogeneity characteristic of the classical geometries, their metrics endow them with the three main structures pertinent to flattening: metric structure, curvature structure, and conformal structure.

*Metric structure*

The Riemannian metric $\rho$ on $S$ is defined by a differential element of arclength d$s$ within each face. Integrating d$s$ along a path gives its length, and the distance $\rho(p,q)$ is the length of the shortest path lying in $S$ and connecting $p$ to $q$. Double integration of d$s$ over a region $\Omega\subset S$ gives its area.

*Curvature structure*

The *curvature* of $S$ has to do with its shape in space. *Gaussian* curvature is used as it depends only on distances within $S$ itself, not on how $S$ lies in $\mathbb{R}^3$. A rounded region, say a hilltop, represents positive curvature; a plain or valley floor is flat, zero curvature; while a saddle point, such as a mountain pass, has negative curvature. Since these surfaces are *piecewise flat*, all the non-zero curvatures reside at the vertices. If $v$ is a vertex and $\theta(v)$ is the sum of the angles at $v$ in all the triangles meeting at $v$, then *curvature* at $v$ is defined to be $2\pi-\theta(v)$. Positive, zero, and negative curvature have their familiar geometric interpretations. For example, a cone point composed of 5 equilateral triangle faces has a total angle sum of $5\pi/3$, giving positive curvature $\pi/3$. Six faces of equilateral triangles demonstrates zero curvature (flat); and a saddle point composed with 8 equilateral faces demonstrates negative curvature $-2\pi/3$.

*Conformal structure*

A mapping is conformal if it preserves angles and angle direction between curves. On piecewise flat surfaces there is a slight subtlety about the meaning of angle for curves that meet at a vertex $v$; namely, one needs a "market share" or proportional interpretation. Suppose $\gamma$ and $\sigma$ are curves that intersect at $v$. As before, let $\theta(v)$ denote the sum of the angles of all the triangles meeting at $v$. Sweeping the tangent vector to $\gamma$ counterclockwise about $v$ within the surface until it is tangent to $\sigma$ will accumulate some turning angle $\beta$ through these faces. The angle between $\gamma$ and $\sigma$ is not $\beta$, but rather is the ratio $\alpha=2\pi\beta/\theta(v)$ which measures $\beta$'s *market share* or proportion of $\theta(v)$. This is really quite natural: if $\beta$ represents, say, a quarter of the total angle at $v$, $\beta=(1/4)\theta(v)$, then under a conformal flattening one would expect the images of $\gamma$ and $\sigma$ to meet in the angle $\alpha=2\pi(1/4)=\pi/2$, that is, in a right angle.

These interpretations of curvature and angle in the piecewise flat setting are entirely standard. They are local, intrinsic to $S$, converge to the usual meanings when piecewise flat surfaces approximate smooth surfaces, and they have exactly the intuitive content one expects.

*Primer on surface maps*

A *mapping* $f$ from one surface, $S_1$, to another, $S_2$, is a *one-to-one function* $f : S_1 \mapsto S_2$. That is, every point $x_1$ of $S_1$ corresponds with a unique point $x_2=f(x_1)$ in $S_2$, and if $x$ and $y$ are distinct points of $S_1$ then $f(x)$ and $f(y)$ are distinct points of $S_2$. Thus $f$ effectively identifies $S_1$ with the subset $f(S_1)$ in $S_2$ so that locations, curves, or regions of $S_1$ are identified with corresponding locations, curves, or regions in $S_2$.

Assuming $S_1$ and $S_2$ have conformal structures, $f$ is *conformal* if it preserves angles and angle direction between curves. Paraphrasing an equivalent and more intuitive condition: $f$ is conformal if for each point $p$ of $S_1$, the images of tiny circles centered at $p$ are tiny (approximate) circles centered at $f(p)$ in $S_2$. This latter condition can be loosened to define the more general class of *quasiconformal* maps: $f$ is $\kappa$-*quasiconformal* if for each point $p$ of $S_1$, the images of tiny circles centered at $p$ are tiny (approximate) *ellipses* centered at $f(p)$ in $S_2$ and having eccentricity bounded by $\kappa$.

There are innumerable equivalent (and precise) definitions of *quasiconformal*; it is a highly developed field in PDE's and in studies of conformal mapping (see Lehto and Virtanen, 1973). The parameter $\kappa$, $\kappa\geq 1$, is one measure of conformal *distortion* of $\kappa$-quasiconformal maps; indeed, $f$ is conformal if and only if it is 1-quasiconformal. Piecewise affine maps are, in practice, never conformal, always quasiconformal. However, $\kappa$ indicates "worst-case" local distortion; in practice, even when $\kappa$ is large a $\kappa$-quasiconformal map $f$ will convey significant conformal information.

*Primer on circle packing*

As defined earlier, a circle packing is a configuration of circles with a specified pattern of tangencies. Here is some standard terminology.

*Complex*

$K$ denotes a *complex* (technically, an abstract simplicial 2-complex) associated with a triangulation of a topological surface. This is basically a "list" of the vertices $v$, edges $\langle v,u\rangle$, and oriented faces $\langle v,u,w\rangle$ of the triangulation, and represents a "pattern".

*Packing*

$P$ denotes a *circle packing* for $K$ in one of the target geometries $\mathcal{T}$. More specifically, $P$ is a collection $\{c_v\}$ of circles, one for each vertex $v$ of $K$, so that $c_v$ is tangent to $c_u$ whenever $\langle v,u\rangle$ is an edge of $K$ and so that the triple $\langle c_v,c_u,c_w\rangle$ of mutually tangent circles is positively oriented in $\mathcal{T}$ whenever $\langle v,u,w\rangle$ is a positively oriented face of $K$.

*Maximal packing*

The essentially unique extremal packing $P_K$ for $K$: if $K$ triangulates a sphere, this is a packing of the Riemann sphere $\mathbb{S}^2$, while if $K$ triangulates a disc, this is a hyperbolic packing whose boundary circles are horocycles (internally tangent to the unit circle), e.g., Fig. 2c.

*Packing label*

$R$ is the collection $\{r_v\}$ of radii, one for each vertex $v$ of $K$, so that $r_v$ is the radius (in the metric of $\mathcal{T}$) for circle $c_v$.

*Angle sum*

Given putative radii for a vertex $v$ and its immediate neighbors, $\theta(v)$ is the sum of angles at $v$ in the faces these form, each computed by the appropriate Law of Cosines. When $v$ is interior, the radii form a flat packing at $v$ if and only if $\theta(v)=2\pi$.

*Carrier*

Carr ($P$) denotes the concrete *geometric triangulation* in $\mathcal{T}$ formed by connecting the centers of tangent circles of $P$ with geodesic segments; this provides a mesh in $\mathcal{T}$ which is combinatorially equivalent to $K$.

Starting with a given topologically correct complex $K$: 1) The complex $K$ is the triangular mesh of some reconstructed cortical surface $S$. 2) The packing $P$ is a circle packing for $K$ guaranteed by the DRMT and the CPT (Beardon and Stephenson, 1990). 3) The packing label $R$ is computed (approximately), giving the circle radii, and the circles are laid out to give $P$. 4) Carr ($P$) is used (as described below) to define the desired flat map $f : S \to \mathcal{T}$. Some of the technical issues involved are:

A) Computational effort lies mainly in approximating a packing label $R$ with iterative methods (see the section on *Computing conformal maps via circle packing*); laying out $P$ is then straightforward. For maximal packings, linearized methods of Orick compute circle radii and centers simultaneously and are much faster (Orick, in preparation).

B) There is (as yet) no packing algorithm intrinsic to spherical geometry. One uses the puncture trick described in the section on *Computing conformal maps via circle packing* so the computations are actually done in $\mathbb{D}$. Other triangulated surfaces can also be packed in $\mathbb{S}^2$, as illustrated in Fig. 4e, but all are projected from $\mathbb{C}$ or $\mathbb{D}$.

C) If $P$ is a circle packing for $K$ in target space $\mathcal{T}$, then each vertex $p$ of $S$ corresponds to a vertex $v \in K$, hence to a circle $c_v \in P$, and hence to its circle center $z_v$ in $\mathcal{T}$. Define $f(p)=z_v$, then extend $f$ to edges, and finally to faces. The result is a simplicial map $f : S \mapsto \mathrm{carr}(P) \subset \mathcal{T}$. This is the "flat" map on $S$ induced by $P$ and is called a *discrete conformal map*. Of course, a different packing $P$ or considering $P$ in a different geometry $\mathcal{T}$ can heavily effect the properties of $f$. On the other hand, details, such as how $f$ was extended to edges and faces, are largely immaterial in practice.

D) The quasiconformal dilatation $\kappa$ for discrete conformal maps is well controlled. *A priori* upper bounds are derived from the key Ring Lemma of (Rodin and Sullivan, 1987) and from lower bounds for the angles in the triangular mesh. In practice, precise bounds for $\kappa$ are not a high priority; intrinsic advantages of the discrete theory outweigh mere approximation of classical maps. In any case, mesh refinements, parallel computation, and introduction of overlap and inversive distance packings (conformally invariant properties, see Bowers and Hurdal, 2003 for details) will further reduce quasiconformal distortion. An overlap packing is illustrated in Fig. 2d.

## References


Ahlfors, L.V., 1966. Complex Analysis. McGraw-Hill Book Company, New York.

Andre'ev, E.M., 1970. Convex polyhedra in Lobacevskii space. Math USSR Sbornik 10, 413–440.

Angenent, S., Haker, S., et al., 1999. On the Laplace–Beltrami operator and brain surface flattening. IEEE T. Med. Imaging 18, 700–711.

Armstrong, M.A., 1983. Basic Topology. Springer-Verlag, New York.

Beardon, A.F., Stephenson, K., 1990. The uniformization theorem for circle packings. Indiana Univ. Math J. 39, 1383–1425.

Bowers, P.L., Hurdal, M.K., 2003. Planar conformal mappings of piecewise flat surfaces. In: Hege, H.-C., Polthier, K. (Eds.), Visualization and Mathematics III. Springer Verlag, Berlin, pp. 3–34.

Collins, C., Stephenson, K., 2003. A circle packing algorithm. Comp. Geom. 25, 21–34.

Crowdy, D.G., 2007. Schwarz–Christoffel mappings to unbounded multiply connected polygonal regions. Math Proc. Camb. Phil. Soc. 142, 319–339.

Csernansky, J.G., Wang, L., et al., 2004. Computational anatomy and neuropsychiatric disease: probabilistic assessment of variation and statistical inference of group difference, hemispheric asymmetry, and time-dependent change. Neuroimage 23, 56–68.

Dale, A.M., Sereno, M.I., 1993. Improved localization of cortical activity by combining EEG and MEG with MRI cortical surface reconstruction: a linear approach. J. Cognitive Neurosci 5, 162–176.

Dale, A.M., Fischl, B., et al., 1999. Cortical surface-based analysis I: segmentation and surface reconstruction. Neuroimage 9, 179–194.

DeLillo, T.K., 2006. Schwarz–Christoffel mapping of bounded, multiply connected domains. Comput. Methods Funct. Theory 6, 275–300.

Drury, H.A., Van Essen, D.C., et al., 1996. Computerized mappings of the cerebral cortex: a multiresolution flattening method and a surface-based coordinate system. J. Cognitive Neurosci. 8 (1), 1–28.

Fary, I., 1948. On straight lines representation of planar graphs. Acta. Sci. Math Szeged 11, 229–233.

Fischer, B., 1973. Overlap of receptive field centres and representation of the visual field in the cat's optic tract. Vision Res. 13, 2113–2120.

Fischl, B., Sereno, M.I., et al., 1999. Cortical surface-based analysis II: inflation, flattening, and a surface-based coordinate system. Neuroimage 9, 195–207.

Goebel, R., 2000. A fast automated method for flattening cortical surfaces. Neuroimage 11, S680 Part 2.

Gu, X., Vemuri, B.C., 2004. Matching 3D shapes using 2D conformal representations. In: Barillot, C., Haynor, D.R., et al. (Eds.), Lect. Notes Comput. Sc. MICCAI 2004, 3216. Springer, Berlin, pp. 771–780.

Gu, X., Wang, Y., et al., 2004. Genus zero surface conformal mapping and its application to brain surface mapping. IEEE T. Med. Imaging 23, 949–959.

Gutman, B., Wang, Y., et al., 2007. Hippocampal surface analysis using spherical harmonic function applied to surface conformal mapping. Proceedings of 4th IEEE International Symposium on Biomedical Imaging (ISBI), pp. 1172–1175.

Hurdal, M.K., 2008. TopoCV software. http://www.math.fsu.edu/~mhurdal.

Hurdal, M.K., Stephenson, K., 2004. Cortical cartography using the discrete conformal approach of circle packings. Neuroimage 23, S119–S128.

Hurdal, M.K., Bowers, P.L., et al., 1999. Quasi-conformally flat mapping the human cerebellum. In: Taylor, C., Colchester, A. (Eds.), Lect. Notes Comput. Sc. . MICCAI'99, 1679. Springer, Berlin, pp. 279–286.

Hurdal, M.K., Lee, A., et al., 2003. Investigating the medial prefrontal cortex with cortical flat mappings. Neuroimage 2 (Suppl. 1), S44 CD–Rom Abstract 856.

Ju, L., Hurdal, M.K., et al., 2005. Quantitative evaluation of three cortical surface flattening methods. Neuroimage 28, 869–880.

Kenyon, R., Okounkov, A., 2007. Limit shapes and the complex burgers equation. Acta Math 199, 263–302.

Koebe, P., 1936. Kontaktprobleme der Konformen Abbildung. Ber Sächs Akad Wiss Leipzig, Math-Phys Kl 88, 141–164.

Lawler, G.F., Schramm, O., et al., 2004. Conformal invariance of planar loop-erased random walks and uniform spanning trees. Ann. Probab. 32, 939–995.

Lehto, O., Virtanen, K.I., 1973. Quasiconformal Mappings in the Plane, Second edn. Springer-Verlag, New York.

Levy, B., Petitjean, S., et al., 2002. Least squares conformal maps for automatic texture atlas generation. Comput. Graph. (Proc SIGGRAPH 02). Addison Wesley.

Lorensen, W.E., Cline, H., 1987. Marching cubes: a high resolution 3D surface construction algorithm. Comput. Graph. 21, 163–169.

Lui, L.M., Thiruvenkadam, S., et al., 2008. Optimized conformal parameterizations of cortical surfaces using shape based matching of landmark curves. MICCAI 2008. Vol. in press of Lect. Notes Comput. Sc. Springer, Berlin.

Lui, L.M., Wang, Y., et al., 2007a. Brain anatomical feature detection by solving partial differential equations on general manifolds. Discrete Cont. Dyn-B. 7, 605–618.

Lui, L.M., Wang, Y., et al., 2007b. Landmark constrained genus zero surface conformal mapping and its application to brain mapping research. Appl. Numer. Math 57, 847–858.

MacDonald, D., Kabsni, N., et al., 2000. Automated 3-D extraction of inner and outer surfaces of cerebral cortex from MRI. Neuroimage 12, 340–355.

Mangin, J.-F., Frouin, V., et al., 1995. From 3D magnetic resonance images to structural representations of the cortex topography using topology preserving deformations. J. Math Imaging Vis. 5, 297–318.

Marshall, D., Rohde, S., 2007. Convergence of a variant of the zipper algorithm for conformal mapping. SIAM J. Numer. Anal. 45, 2577–2609.

Massey, W.S., 1967. Algebraic Topology: An Introduction. Springer-Verlag, New York.

Murray, J.D., 1989. Mathematical Biology. Springer-Verlag, Berlin. chapter 16.

Nie, J., Liu, T., et al., 2007. Least-square conformal brain mapping with spring energy. Comput. Med. Imag. Graph. 31, 656–664.

Orick, G. in preparation. A linearized circle packing algorithm.

Polya, G., 1968. Mathematical Discovery, 2. John Wiley and Sons, New York.

Qui, A., Rosenau, B.J., et al., 2006. Estimating linear cortical magnification in human primary visual cortex via dynamic programming. Neuroimage 31, 125–138.

Ratnanather, J.T., Barta, P.E., et al., 2003. Dynamic programming generation of boundaries of local coordinatized submanifolds in the neocortex: application to the planum temporale. Neuroimage 20, 359–377.

Ratnanather, J.T., Botteron, K.N., et al., 2001. Validating cortical surface analysis of medical prefrontal cortex. Neuroimage 14, 1058–1069.

Rehm, K., Lakshminaryan, K., et al., 1998. A symbolic environment for visualizing activated foci in functional neuroimaging datasets. Med. Image Anal. 2, 215–226.
Rehm, K., Rottenberg, D., et al., 2000. Use of cerebellar landmarks to define a coordinate system and an isolation strategy. Neuroimage 11, S536 Part 2.
Riemann, B., 1876. Grundlagen für eine allgemeine theorie der functionen einer veränderlichen complexen grösse, inauguraldissertation, göttingen, 1851, Gesammelte mathematische Werke und wissenschaftlicher Nachlass, 2nd. Teubner, Leipzig, pp. 3–48.
Rodin, B., Sullivan, D., 1987. The convergence of circle packings to the Riemann mapping. J. Differ. Geom. 26, 349–360.
Rosa, M.G.P., Fritsches, K.A., et al., 1997. The second visual area in the marmoset monkey: visuotopic organisation, magnification factors, architectonical boundaries, and modularity. J. Comp. Neurol. 387, 547–567.
Schmahmann, J.D., Doyon, J., et al., 1999. Three-dimensional MRI atlas of the human cerebellum in proportional stereotaxic space. Neuroimage 10, 233–260.
Schroeder, W., Martin, K., et al., 1998. The Visualization Toolkit. Prentice Hall, Upper Saddle River, NJ.
Schwartz, E.L., 1980. Computational anatomy and functional architecture of striate cortex: a spatial mapping approach to perceptual coding. Vision Res. 20, 645–669.
Schwartz, E.L., 1989. A numerical solution to the generalized mapmaker's problem: flattening nonconvex polyhedral surfaces. IEEE T. Pattern Anal. 11, 1005–1008.
Schwartz, E.L., 1994. Computational studies of the spatial architecture of primate visual cortex. In: Peters, A., Rockland, K.S., Cronly-Dillon, J.R. (Eds.), Cerebral Cortex. Primary Visual Cortex in Primates, 10. Plenum Press, New York, pp. 375–395. chapter 9.
Shattuck, D.W., Leahy, R.M., 2002. Brainsuite: an automated cortical surface identification tool. Med. Image Anal. 8, 129–142.
Stephenson, K., 1992–2008. CirclePack software. http://www.math.utk.edu/~kens.
Stephenson, K., 1999. Approximation of conformal structures via circle packing. In: Papamichael, N., Ruscheweyh, S., et al. (Eds.), Computational Methods and Function Theory 1997, Proc Third CMFT Conference, 11. World Scientific, pp. 551–582.
Stephenson, K., 2002. Circle packing and discrete analytic function theory. In: Kühnau, R. (Ed.), Handbook of Complex Analysis, Vol. 1: Geometric Function Theory. Elsevier, Amsterdam.
Stephenson, K., 2005. Introduction to Circle Packing and the Theory of Discrete Analytic Functions. Camb. Univ. Press.
Thompson, P.M., Hayashi, K.M., et al., 2004. Mapping cortical change in Alzheimer's disease, brain development, and schizophrenia. Neuroimage 23, S2–S18.
Thurston, W., 1985. The finite Riemann mapping theorem. Invited talk, An International Symposium at Purdue University on the occasion of the proof of the Bieberbach conjecture, March 1985.
Thurston, W., 1997. The Geometry and Topology of 3-Manifolds. Princeton University Press, Princeton, NJ.
Toga, A.W., Mazziotta, J.C. (Eds.), 1996. Brain Mapping: The Methods. Academic Press, Inc., San Diego.
Tosun, D., Rettmann, M.E., et al., 2006. Cortical reconstruction using implicit surface evolution: accuracy and precision analysis. Neuroimage 29, 838–852.
Tusa, R.J., Palmer, L.A., et al., 1978. The retinotopic organization of area 17 (striate cortex). J. Comp. Neurol. 177, 213–236.
Van Essen, D.C., Drury, H.A., et al., 1998. Functional and structural mapping of human cerebral cortex: solutions are in the surfaces. Proc. Natl. Acad. Sci. U. S. A. 95, 788–795.
Wagner, K., 1936. Bemerkunge zum Vierfarbenproblem. Jber Deutsch Math-Verein 46, 26–32.
Wandell, B.A., Chial, S., et al., 2000. Visualization and measurement of the cortical surface. J. Cognitive Neurosci. 12, 739–752.
Wang, Y., Chiang, M.C., et al., 2005. Automated surface matching using mutual information applied to Riemann surface structures. In: Duncan, J., Gerig, G. (Eds.), Lect. Notes Comput. Sc. . MICCAI 2005, 3749. Springer, Berlin, pp. 666–674.
Wang, Y., Gu, X., et al., 2006. Brain surface conformal parameterization with algebraic functions. In: Larsen, R., Nielsen, M., et al. (Eds.), Lect. Notes Comput. Sc. . MICCAI 2006, 4191. Springer, Berlin, pp. 946–954.
Wang, Y., Lui, L.M., et al., 2007. Brain surface conformal parameterization using Riemann surface structure. IEEE T. Med. Imaging 26, 853–865.
Wood, Z., Hoppe, H., et al., 2004. Removing excess topology from isosurfaces. ACM T. Graphic 23, 190–208.